JOURNAL OF SPACECRAFT AND ROCKETS
Vol. 36, No. 4, July–August 1999

# Friction Model of a Revolute Joint for a Precision Deployable Spacecraft Structure

M. Roman Hachkowski*
*Raytheon Optical Systems, Danbury, Connecticut 06810*
Lee D. Peterson†
*University of Colorado, Boulder, Colorado 80309-0429*
and
Mark S. Lake‡
*NASA Langley Research Center, Hampton, Virginia 23681*

**An analytical model is presented for predicting breakaway friction torque in a precision deployable spacecraft structure joint incorporating preloaded angular contact bearings. The model is based on the Todd/Johnson tribological friction model of friction within ball bearings (Todd, M. J., and Johnson, K. L., "A Model for Coulomb Torque Hysteresis in Ball Bearings," *International Journal of Mechanical Science*, Vol. 29, 1987, pp. 339–354) and includes the effects of Coulombic microslippage between the bearing components and material hysteretic damping. A new nondimensional parameter is developed to quantify the effects of bearing preload, geometry, and material properties. It is analytically shown that bearing friction can be minimized for a specific bearing contact angle considering both rolling and sliding friction components. Additionally, steady-state bearing friction is calculated to vary nonlinearly with assembly preload. Analytical prediction of bearing friction is correlated with measured data.**

## Nomenclature

| | |
|---|---|
| $A_{1,2,3}$ | = nondimensional constants |
| $a$ | = semiminor axis of the Hertzian contact ellipse, m |
| $b$ | = semimajor axis of the Hertzian contact ellipse, m |
| $C_{ri}$, $C_{ro}$, $C_z$ | = constants that define the contribution of conformity and spin friction |
| $c$ | = conformity ratio, $r_g/r_b$ |
| $E$ | = Young's modulus, Pa |
| $F$ | = tangential forces that are developed at the points of contact between a race and a ball, N |
| $g$ | = gravitational acceleration, m/s$^2$ |
| $I$ | = mass moment of inertia of the moving joint half, kg m$^2$ |
| $K$ | = single bearing compression scale parameter |
| $k$ | = constants that are functions of the elastic bodies' material properties |
| $M_h$ | = hysteretic friction torque, Nm |
| $M_r$ | = conformity Heathcote[17] friction torque, Nm |
| $M_z$ | = spin friction torque, Nm |
| $m_j$ | = moving joint half mass, kg |
| $n_b$ | = number of ball bearings in the bearing set |
| $P$ | = normal load on a single ball bearing, N |
| $p(x)$ | = Hertzian pressure distribution, Pa |
| $p_0$ | = maximum pressure of the Hertzian pressure distribution, Pa |
| $R_i$, $R_o$ | = inner or outer radius to the point of contact between a ball and the inner or outer race, m |
| $r_b$ | = radius of an individual ball, m |
| $r_{cg}$ | = radius from the center of rotation to the center of gravity of the moving joint half, m |
| $r_{ei}$ | = radial dimension parameter [see Eq. (16)] |
| $r_g$ | = radius of the race grove, m |
| $T_{ss}$ | = applied torque about the bearing axis to overcome resistance to motion, Nm |
| $x$ | = local Cartesian coordinate along semiminor axis within contact ellipse |
| $y$ | = local Cartesian coordinate along semimajor axis within contact ellipse |
| $\alpha$ | = material hysteresis loss factor |
| $\beta$ | = contact angle of the bearing set, rad |
| $\Delta\omega_z$ | = difference in rotation rates between inner race and ball [see Eq. (14)] |
| $\varepsilon$ | = roll/spin parameter |
| $\eta$ | = nondimensionalized coordinate along semimajor axis within contact ellipse, $y/b$ |
| $\theta$ | = breakaway angle |
| $\mu_s$ | = sliding coefficient of friction |
| $\nu$ | = Poisson's ratio |
| $\xi$ | = microslip parameter |
| $\tau_F$ | = surface tractions that create coupled moments, Pa |
| $\tau_t$ | = total surface tractions, Pa |
| $\tau_0$ | = surface tractions that create frictional sliding forces, Pa |
| $\omega_i$ | = angular velocity of a inner bearing race |
| $\omega_{rb}$ | = angular velocity of a single ball in the roll direction |
| $\omega_{zb}$ | = angular velocity of a single ball in the spin direction |

Presented as Paper 96-1472 at the AIAA/ASME/ASCE/AHS/ASC 37th Structures, Structural Dynamics, and Materials Conference, Salt Lake City, UT, 15–17 April 1996; received 21 November 1996; revision received 11 November 1998; accepted for publication 21 November 1998. Copyright © 1999 by the authors. Published by the American Institute of Aeronautics and Astronautics, Inc., with permission.

*Senior Engineer, Space and Strategic Programs; mrhachkowski@west.raytheon.com. Member AIAA.

†Associate Professor, Center for Aerospace Structures, Department of Aerospace Engineering Sciences; lee.peterson@colorado.edu. Senior Member AIAA.

‡Research Engineer, Structural Mechanics Branch; m.s.lake@larc.nasa.gov. Senior Member AIAA.

## Introduction

SPACECRAFT designers have always used deployable structures to reduce the packaged volume of the spacecraft. Many low-precision components, such as appendage booms, and moderate-precision components, such as communication antennas, have been successfully deployed in space. All of these devices have incorporated joint and latch mechanisms whose structural response is nonlinear and complex, involving numerous localized phenomena that are difficult to model. Historically, these nonlinear response characteristics have been treated as uncertainties requiring large design factors of safety. For example, values for friction torque within revolute, i.e., hinge, joints are often estimated by applying factors of safety of three or more to upper bounds on test data from

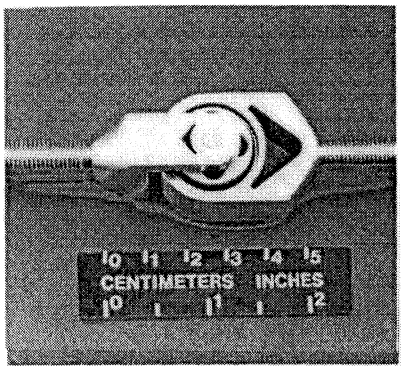


**Fig. 1 High-precision, low-friction, zero-freeplay hinge joint.**

similar mechanisms.[1–3] Such estimates can be very conservative and lead to oversized deployment actuation systems.[4–6] However, these inefficiencies are tolerated in the design of low- and moderate-precision deployable structures to avoid the complexity of developing detailed models of the friction behavior.

Recently, significant interest has developed in the design of high-precision deployable structures for scientific instruments, such as large telescope mirrors and interferometer booms.[7] A revolute joint, which exhibits highly linear response under load cycling, has been developed for application to these high-precision deployable structures.[8] This joint (Fig. 1) eliminates common sources of nonlinear load-cycling response and kinematic imprecision by incorporating a preloaded angular contact bearing in place of a conventional pin.[9,10] Like all rolling element bearings, angular contact bearings consist of two races (the inner race and the outer race), a set of rolling elements, e.g., balls, and a separator (usually called a cage or retainer). The separator is used for keeping the set of rolling elements equally spaced. Although angular contact bearings find common use in articulated optics and steering mirrors, their use in load bearing truss structures is new.

One of the potential advantages of these precision revolute joints is the ability to model analytically the friction torque as a function of key design parameters. If such a model could be developed, it would lead to more reliable deployments because of predictable actuation torque power. In addition, recent testing on a prototype deployable telescope metering structure that incorporates these new joints has identified micron-level dimensional instabilities that are correlated with friction in the joints.[11] To understand the relationship between component-level friction and dimensional instability better and to enable significant advancements in the design of high-precision deployable structures, it is necessary to develop better analytical models of frictional behavior.

The determination of the friction torque in rolling element bearings has been a topic of research for the past 50 years.[12] Much of this research applies only to high-speed applications, e.g., 10,000 rpm, and is inapplicable to space deployment applications, for which rotational velocities can be ~0.5 deg/s (Ref. 13). However, there exists a small body of work that focuses on the quasistatic contact mechanics of two rolling bodies. This work has identified three distinct friction mechanisms that occur when two bodies roll past each other.[14–18]

Palmgren[19] published the first work that described friction due to conformity between the balls and races in a ball bearing. Heathcote[17] analytically derived the friction contribution of conformity surface tractions. Poritsky et al.[20] provided the earliest work on recognizing friction torque due to spinning of the balls. Johnson[14] provided the current theory of microslip derived spin friction torque. Tabor[18] derived a theory of rolling friction due to viscous hysteresis in the bearing material. Halling[15,16] attempted to derive microslip with spin patterns in ball-thrust bearings. He verified that friction due to a spin/roll condition is smaller than when complete slip occurs.

Todd and Johnson[21] were the first to derive an analytical model for predicting friction within ball bearings including the effects of all three friction mechanisms: spinning of the balls, conformity between the balls and the races, and viscous hysteresis. For angular contact bearings, two of the friction mechanisms, i.e., spinning friction and conformity friction, are coupled and are difficult to resolve. The differentiation of these friction components primarily relies on the assumed kinematic distribution of sticking and slipping within the Hertzian contact patch of individual ball bearings. For this reason, application of the Todd/Johnson model requires further validation, such as that provided by this paper. Prior to the present study, the Todd/Johnson model had been verified only for three-ball-bearing systems.[21]

In the present study, the Todd/Johnson model is applied to predict analytically the steady-state friction torque within the precision revolute joint angular contact bearing set. The goals of this study are 1) to evaluate of the Todd/Johnson analytical friction model for predicting friction torque within an angular contact bearing; 2) to develop a nondimensional analysis that defines the dependencies of the friction torque on joint geometry, material properties, and preload; 3) to correlate the model predictions with data from breakaway friction testing of a prototype precision revolute joint; and 4) to discuss how the new friction torque model can be used in the design of revolute joints for high-precision deployable structures. The principle contributions of this paper are the validation of the Todd/Johnson model on the breakaway friction of a multiple bearing set and the development of nondimensional scaling parameters for joint friction minimization.

## Analytical Modeling of Angular Contact Bearings

### Friction Mechanisms Within an Angular Contact Bearing

As a bearing slowly accelerates from a rest condition to a uniform angular velocity, the resisting torque does not instantly jump to its final value but approaches the steady rolling torque asymptotically through a small angle of rotation (<0.2 deg). When the rolling direction of the bearing is reversed after achieving a steady rolling state, the same behavior (beginning at a low-level torque and slowing approaching a steady rolling torque) is observed. Dahl[22] empirically identified this characteristic behavior. He identified a curve fit expression as well as the two parameters that define the shape of the behavior: the reverse slope, i.e., the slope $s$ immediately following a reversal of direction, and the steady rolling torque $T_{ss}$. All of his work concentrated on empirically identifying the correct function that accurately describes this phenomenon.

More recent analyses, like that developed by Todd and Johnson,[21] have proven microslip between the bearings and the races to be the dominate source of hysteretic response. The Todd/Johnson model includes the following three mechanisms for predicting ball-bearing friction torque: microslip from the angular velocity of spin of the balls relative to the race; microslip due to conformity between the balls and the race, often referred to as Heathcote[17] slip; and material viscous hysteresis arising from stress cycling in the material due to the rolling of the balls traveling across the race.

#### *Microslip Friction Due to Spin*

When an angular contact bearing set rotates, the individual balls both spin and roll about their vertical and horizontal axes relative to the races. For the balls to spin, microslipping must occur between the ball and race, and surface tractions due to friction must develop. The distribution of surface tractions in the Hertzian contact ellipse due to spinning of the ball is shown in Fig. 2. These surface tractions give rise to both a moment resultant normal to the plane of the contact ellipse and a force resultant within the plane of the contact ellipse. These force and moment resultants both contribute to a torque that

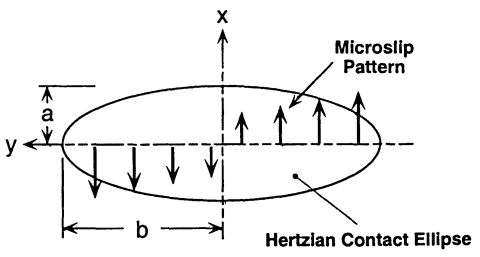


**Fig. 2 Microslip due to spin.**

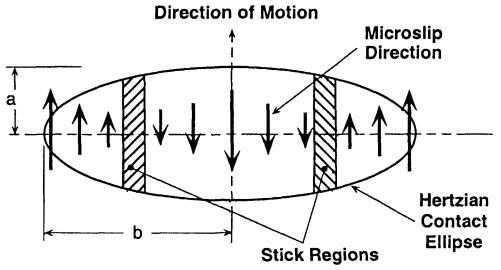


Fig. 3 Microslip due to conformity of the ball bearing and race.

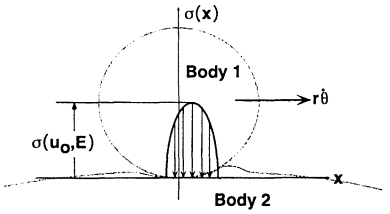


Fig. 4 Stress field due to rolling of one elastic body over another.

resists rotation of the bearing. Johnson[14] determined the friction torque arising from spin-related microslip to be

$$M_z = 0.375\mu_s Pb \tag{1}$$

The essential formulations of Hertzian contact stresses are presented in the Appendix for completeness.

*Microslip Friction Due to Conformity*

Conformity microslip, also called Heathcote slip,[23] arises from the contact area between the ball and the race not being planar due to the transverse curvature of the race. Because of this condition, points in different transverse positions within the contact ellipse are at different radial distances from the center of rotation of the joint and, thus, have different speeds during rotation of the joint. The surface tractions that occur within the Hertzian contact ellipse due to conformity are shown in Fig. 3.

Heathcote[17] developed a theory to predict conformity-induced friction torque by assuming perfect slipping occurs outside of the stick regions, i.e., neglecting the effects of elastic compliance of the ball and race. The Palmgren–Heathcote equation for conformity-induced frictional torque $M_r$ is

$$M_r = 0.0405(\mu_s P)\left(b^2/r_b\right)[(1+c)/c] \tag{2}$$

The frictional moment due to conformity is a nonlinear function of $P$ because the Hertzian contact ellipse dimension $b$ also depends on $P$.

*Hysteretic Rolling Friction*

Rolling is defined as a relative angular motion between two bodies in contact about an axis parallel to their common tangent plane. When rolling occurs without sliding or spinning, the motion is often referred to as pure rolling. The terms free rolling and tractive rolling are used to describe motions in which the tangential force at the contact point of the two bodies is zero and nonzero, respectively. An elastic body in freely rolling contact undergoes a cycle of loading and unloading as it flows through the region of contact deformation. The strain energy of the material in front of the center of contact increases as the center of contact is approached due to the work of compression done by the contact pressure acting on the front-half of the contact area. After the center of contact is passed, the strain energy decreases, and work is done against the contact pressure at the back of the contact. The compressive stress field (and corresponding strain-energy field) that arises between the ball and the race during rolling contact is shown in Fig. 4.

Because of material hysteresis, asymmetry is induced in the compressive contact stress field when a ball rolls, which gives rise to a moment that resists rotation of the ball (Fig. 5). An expression for this moment due to material hysteresis is[18]

$$M_h = \tfrac{3}{16}\alpha Pa \tag{3}$$

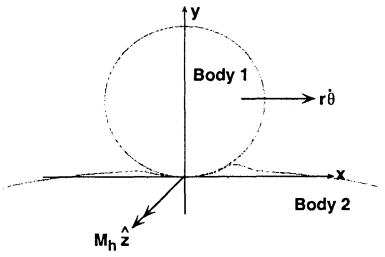


Fig. 5 Resistive moment due to the asymmetry of the pressure field.

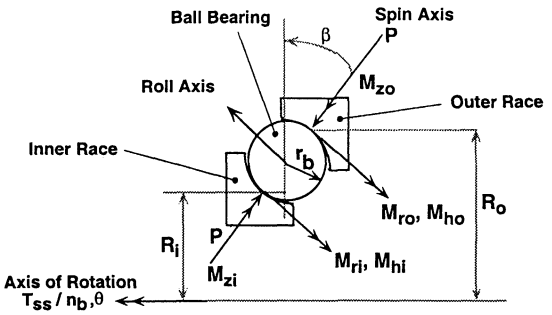


Fig. 6 Forces and moments acting on a ball in an angular contact bearing.

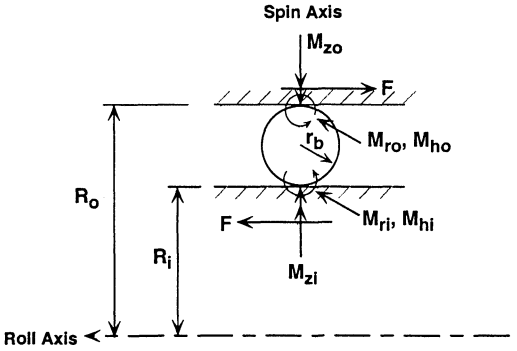


Fig. 7 Forces and moments acting in a plane defined by the ball bearing.

Similar to the conformity moment, the hysteresis moment is a nonlinear function of $P$ because the Hertzian ellipse dimension $a$ also depends on $P$.

**Coupled Friction Mechanics in an Angular Contact Ball Bearing**

In an angular contact bearing, the distribution of sticking and slipping regions within the contact area means that the spin and conformity friction components are coupled. The derivation of spin and conformity friction contributions is Todd and Johnsons'[21] contribution. The authors have reviewed and expounded on Todd and Johnsons' derivation to clarify the underlying assumptions of their analysis.

As presented by Todd and Johnson,[21] the total friction in a bearing is based on the static equilibrium of an individual ball. Moments and forces that are present at the interfaces between the balls and the inner and outer races are shown in Fig. 6. Figure 6 is a cross-sectional cut through the inner and outer races and a single ball of the bearing. Note that both moments and force resultants arise from the tangential friction stress at the interfaces. In this reference frame, the only force resultant that appears is the contact normal force $P$. The forces and moments in a plane perpendicular to the plane shown in Fig. 6 and which contains the spin axis of the ball are shown in Fig. 7. In this reference frame, an additional force resultant $F$ appears, which is the result of microslip-induced tractions arising from both spin and conformity of the ball.

Assuming that the bearings are in a steady-state rolling condition, i.e., neglect D'Alembert inertia forces, the equilibrium equation for a single ball about its spin axis is

$$M_{zi} - M_{zo} = 0 \tag{4}$$

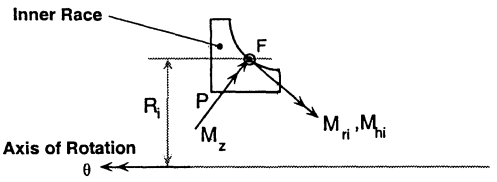


**Fig. 8 Forces acting on the inner race.**

or

$$M_{zi} = M_{zo} = M_z \tag{5}$$

The equilibrium torque equation about the roll axis is

$$M_{ri} + M_{ro} + M_{hi} + M_{ho} = 2r_b F \tag{6}$$

$M_{ri}$, $M_{ro}$ and $M_{hi}$, $M_{ho}$ are not the same values because the contact area of the two contact surfaces (bearing contacting with the inner and outer races) are of different dimensions.

Equations of equilibrium can also be derived for the inner race of the bearing to determine the external torque necessary to overcome the rolling resistance of the balls. Referring to Fig. 8 (note that $F$ is directed out of the page) and again neglecting inertia, the equilibrium equation for moments about the axis of rotation is

$$T_{ss}/n_b = M_z \sin\beta + M_{ri}\cos\beta + M_{hi}\cos\beta + FR_i \tag{7}$$

From Fig. 6,

$$\cos\beta = \frac{R_o - R_i}{2r_b} \tag{8}$$

From Eq. (6),

$$F = \frac{M_{ri} + M_{ro} + M_{hi} + M_{ho}}{2r_b} \tag{9}$$

Substituting Eqs. (8) and (9) into Eq. (7) results in the following equation:

$$\frac{T_{ss}}{n_b} = M_z \sin\beta + \left(\frac{M_{ri}R_o + M_{ro}R_i}{2r_b}\right) + \left(\frac{M_{hi}R_o + M_{ho}R_i}{2r_b}\right) \tag{10}$$

Equation (10) gives the steady-state friction torque needed to overcome the rolling resistance of the bearing. It includes contributions from the three friction mechanisms identified earlier. The first term is the spin friction torque contribution; the second term is the Heathcote, i.e., conformity, friction torque contribution; the third term is the hysteretic friction torque contribution.

The basis of the Todd/Johnson derivation is the relation of these force and moment results to the distribution of slip and stick regions within the contact patch. The underlying assumption (introduced by Palmgren[19] and Heathcote[17]) is that surface tractions only develop as a consequence of microslipping between the balls and the races, i.e., it is assumed that static friction is insignificant. More specifically, it is assumed that surface tractions are aligned with the direction of microslipping and proportional to the normal pressure and the sliding friction coefficient between the contacting surfaces. Additionally, it is assumed that microslipping (and, consequently, surface tractions) only occurs in the direction of rotation of the ball, i.e., parallel to the semiminor axis of the Hertzian contact ellipse as shown in Fig. 3.

The distribution of microslipping is considered first. Expressions for the velocities of the ball and the races in the direction of rolling, i.e., $x$ direction in Fig. 7, can be derived from geometric considerations. Referring to Fig. 7, the velocity of a point on the surface of the ball located in the contact ellipse is

$$v_b(y) = \omega_{rb}\left[r_b - \left(y^2/2r_b\right)\right] + \omega_{zb}y \tag{11}$$

and the velocity of a corresponding point on the inner race is

$$v_i(y) = \omega_i\left[R_i + \frac{y^2\cos\beta}{2r_b c_i} + y\sin\beta\right] \tag{12}$$

where $\omega_{rb}$ is the angular velocity of the ball in the roll direction, i.e., around the $y$ axis; $\omega_{zb}$ is the angular velocity of the ball in the spin direction, i.e., around the $z$ axis; $\omega_i$ is the angular velocity of a inner bearing race around the rotational axis of the bearing set; and $c_i$ is the inner conformity ratio ($c_i = r_g/r_b$).

Microslip between the ball and the inner race can now be defined mathematically as the difference between the velocities of points in contact with one another on the ball and the inner race. This difference in velocities can be expressed nondimensionally as

$$\xi(\eta) = \frac{(v_b - v_i)}{\omega_i R_i} \tag{13}$$

where $\omega_i R_i$ is the velocity of the inner race along the semiminor axis of the contact ellipse, i.e., the $x$ axis. Substituting Eqs. (11) and (12) into Eq. (13) and rearranging gives

$$\xi(\eta) = \xi_o + \frac{\Delta\omega_{zi} b\eta}{\omega_i R_i} - \frac{b^2\eta^2}{2r_b r_{ei}} \tag{14}$$

where

$$\xi_o = \frac{(\omega_{rb}r_b - \omega_i R_i)}{\omega_i R_i} \tag{15}$$

$$\eta = y/b, \qquad \Delta\omega_{zi} = \omega_{zb} - \omega_i\sin\beta$$
$$1/r_{ei} = (1/R_i)[(\omega_{zb}/\omega_i) + (\cos\beta/c_i)] \tag{16}$$

In general, Eq. (14) has two roots, i.e., two values of $\eta$ for which $\xi(\eta) = 0$. These roots define the regions in which no microslipping occurs (see Fig. 3). Setting Eq. (14) equal to zero and solving for $\eta$ gives

$$\xi_o + \frac{\Delta\omega_{zi} b\eta}{\omega_i R_i} - \frac{b^2\eta^2}{2r_b r_{ei}} = 0 \tag{17}$$

$$\therefore \eta_{1,2} = \frac{\Delta\omega_{zi} r_b r_{ei}}{b\omega_i R_i} \pm \sqrt{\left(\frac{\Delta\omega_{zi} r_b r_{ei}}{b\omega_i R_i}\right)^2 + 2\left(\frac{r_b r_{ei}}{b^2}\right)\xi_o} \tag{18}$$

Performing a simplification,

$$\varepsilon = \frac{\Delta\omega_{zi} r_b r_{ei}}{b\omega_i R_i}, \qquad \delta = \sqrt{\varepsilon^2 + 2\left(\frac{r_b r_{ei}}{b^2}\right)\xi_o} \tag{19}$$

$$\therefore \eta_{1,2} = \varepsilon \pm \delta \tag{20}$$

The way the zones of surface tractions change due to different values of $\varepsilon$ is shown in Fig. 9.

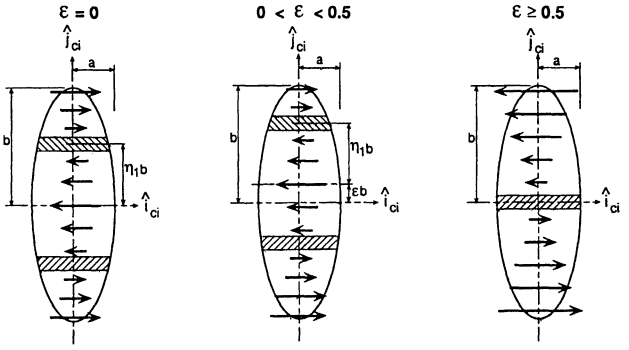


**Fig. 9 Microslip patterns.**

Surface tractions that develop as a consequence of microslipping are now considered. As already explained, it is assumed that surface tractions act opposite to the direction of microslipping and are proportional to the normal pressure and the sliding friction coefficient between the contacting surfaces. Equation (14) gives the direction of microslipping within the contact ellipse, and so an expression for the normal pressure distribution is the only remaining component needed. Following the derivation of Hertz, the Todd/Johnson[21] derivation assumes the normal pressure distribution within the contact ellipse is elliptical. Thus, the Todd/Johnson surface traction distribution is

$$\tau_t(x, y) = -\operatorname{sgn}\xi(y)\mu_s p_0[1 - (x/a)^2 - (y/b)^2]^{\frac{1}{2}} \tag{21}$$

where the sign of $q(x, y)$ is opposite to that of the microslip given by Eq. (14).

Moment resultants can now be derived from Eq. (21) by integrating the tractions throughout the contact ellipse. First the tractions are integrated along a thin strip at constant $y$ using the following force resultant definition:

$$Q_{\text{strip}}(y) = \int_{-x_1}^{x_1} [\tau_t(x, y)]\,dx \tag{22}$$

where

$$x_1 = a(1 - \eta^2)^{\frac{1}{2}} \tag{23}$$

Substituting Eq. (23) into Eq. (22) and integrating gives

$$Q_{\text{strip}}(\eta) = -\operatorname{sgn}\xi(\eta)\mu_s(3P/4b)(1 - \eta^2) \tag{24}$$

Now $Q_{\text{strip}}(\eta)$ can be integrated along $\eta$ to give spin and conformity moment resultants. The spin friction moment is given by

$$M_z = b\int_{-1}^{1} Q_{\text{strip}}(\eta)\eta\,d\eta \tag{25}$$

Performing this integration requires evaluation of sgn $\xi(\eta)$. Referring to Eqs. (17) and (18), the positions of the no-slip bands $\eta_1$ and $\eta_2$ define the points at which $\xi(\eta)$ changes sign. Considering this, it can be shown that

$$M_z/\mu_s Pb = C_z = \tfrac{3}{4}\{\eta_1^2[1 - (\eta_1^2/2)] - \eta_2^2[1 - (\eta_2^2/2)]\} \tag{26}$$

The conformity friction moment that acts on the ball bearing is given by

$$M_r = b^2\int_{-1}^{1} Q_{\text{strip}}(\eta)\left(\frac{\eta^2}{2r_b}\right)d\eta \tag{27}$$

where the radius of the curvature for the Hertzian contact ellipse is approximately $r_b$. Integrating Eq. (27) results in

$$\frac{M_r r_b}{\mu_s Pb^2} = \frac{1}{4}\left[\frac{2}{5} + \eta_2^3\left(1 - \frac{3\eta_2^2}{5}\right) - \eta_1^3\left(1 - \frac{3\eta_1^2}{5}\right)\right] \tag{28}$$

Recall that $\eta_1$ and $\eta_2$ are defined in terms of the parameter $\varepsilon$, which is a function of bearing spin magnitude, i.e., Eq. (18). When $\varepsilon = 0$, the bearing is rolling, i.e., $\Delta\omega_{zi} = 0$. Therefore, the source of friction is due to conformity, $\eta_1 = \delta$ and $\eta_2 = -\delta$, and Eq. (28) reduces to

$$\frac{M_r r_b}{\mu_s Pb^2} = 0.08 \tag{29}$$

which is Heathcote's[17] result [Eq. (2) assuming $c \approx 1$].

When $\varepsilon \geq 0.5$, the bearing primarily is spinning about its own axis and all of the friction is due to the spin friction moment $M_z$. Equation (28) approaches zero, and Eq. (26) equals

$$\lim_{\varepsilon \geq 0.5} \frac{M_z}{\mu_s Pb} = 0.375 \tag{30}$$

Equation (30) is Johnson's[14] equation [Eq. (1)], which predicts the friction caused by a ball spinning on its own axis, i.e., slip occurs over a large proportion of the contact area.

Equations (26) and (28) can be used to derive expressions for spin and conformity moments occurring on both the inner and outer bearing races. Performing these calculations and using Eq. (3) to calculate the hysteretic moment give

$$M_z = C_z\mu_s Pb \tag{31}$$

$$M_{ri} = C_{ri}\frac{\mu_s Pb^2}{r_b}, \qquad M_{ro} = C_{ro}\frac{\mu_s Pb^2}{r_b} \tag{32}$$

$$M_{hi} = \tfrac{3}{16}\alpha Pa_i, \qquad M_{ho} = \tfrac{3}{16}\alpha Pa_o \tag{33}$$

where

$$C_{ri} = \frac{1}{4}\left[\frac{2}{5} + \eta_{2i}^3\left(1 - \frac{3\eta_{2i}^2}{5}\right) - \eta_{1i}^3\left(1 - \frac{3\eta_{1i}^2}{5}\right)\right]$$
$$C_{ro} = \frac{1}{4}\left[\frac{2}{5} + \eta_{2o}^3\left(1 - \frac{3\eta_{2o}^2}{5}\right) - \eta_{1i}^3\left(1 - \frac{3\eta_{1o}^2}{5}\right)\right] \tag{34}$$

Substituting these results into Eq. (10) gives the following expression for the total friction torque resisting rolling within an angular contact bearing:

$$\frac{T_{ss}}{n_b} = C_z\mu_s Pb\sin\beta + \frac{1}{2}\frac{\mu_s Pb^2}{r_b^2}(C_{ri}R_o + C_{ro}R_i) + \frac{3}{32}\frac{\alpha P}{r_b}(a_i R_o + a_o R_i) \tag{35}$$

## Scaling Analysis of Joint Friction Torque

Equation (35) can be nondimensionalized by first normalizing torques by $Pr_b$ and normalizing lengths by $r_b$. The resulting equation is

$$(1/n_b)(T_{ss}/Pr_b) = A_1 K^{\frac{1}{3}}[c/(c-1)]^{\frac{1}{3}}[1 - \nu^2]^{\frac{1}{3}} + A_2\left\{K^{\frac{1}{3}}[c/(c-1)]^{\frac{1}{3}}[1 - \nu^2]^{\frac{1}{3}}\right\}^2 + A_3 K^{\frac{1}{3}}[1 - \nu^2]^{\frac{1}{3}} \tag{36}$$

where

$$A_1 = 1.1447\mu_s(C_z\sin\beta), \qquad A_2 = 0.655\mu_s\left(C_{ri}\frac{R_o}{r_b} + C_{ro}\frac{R_i}{r_b}\right) \tag{37}$$
$$A_3 = 0.108\alpha\left\{\left[\frac{R_i/r_b}{1 + (R_i/r_b)}\right]^{\frac{1}{3}}\frac{R_o}{r_b} + \left[\frac{R_o/r_b}{(R_o/r_b) - 1}\right]^{\frac{1}{3}}\frac{R_i}{r_b}\right\}$$

and a new nondimensional parameter, referred to as the bearing compression parameter, is defined to be

$$K = P/Er_b^2 \tag{38}$$

This parameter quantifies the compressibility of a bearing given a normal load acting on the bearing, bearing material, and geometry. Another nondimensional ratio, referred to as the conformity ratio (as derived by Heathcote[17]), is the following:

$$c = r_g/r_b \tag{39}$$

By normalizing the steady-state friction torque, one can see that the steady-state friction torque is a function of eight nondimensional parameters:

$$(1/n_b)(T_{ss}/Pr_b) = f(K, [1-\nu^2], c, \mu_s, \alpha, \beta, R_i/r_b, R_o/r_b) \tag{40}$$

The nondimensional analysis provides, for design purposes, the ability to 1) compare friction torque characteristics of different bearing arrangements and 2) perform trade studies between different

preloads and bearing arrangements to minimize the friction torque for specific applications. Two design parameters, the applied preload and the contact angle, are the most important parameters over which the designer typically has freedom. The effect of each of these design parameters on the steady-state friction torque is examined next. For purposes of this study, the nominal design parameters are taken to be the parameters of the precision revolute hinge joint listed in Table 1.

The relationship between angular contact bearing angle and nondimensional friction torque for a given nominal preload is shown in Fig. 10. This graph illustrates that for a given preload there is an optimal angular contact bearing angle. As the bearing angle increases, the rolling friction component decreases due to lower normal load $P$. The spinning component, however, has an increased sliding friction component. The optimum angle occurs when the two frictions are balanced. Note from Fig. 10 that the minimum angular contact bearing angle increases as the preload increases. For

**Table 1 Physical parameters of the precision revolute joint**

| Parameter | Symbol | Value |
|---|---|---|
| Young's modulus | $E$ | $200 \times 10^9$ Pa |
| Poisson's ratio | $\nu$ | 0.3 |
| Inner race radius | $R_i$ | $8.9 \times 10^{-3}$ m |
| Bearing diameter | $r_b$ | $7.8 \times 10^{-4}$ m |
| Grove radius | $r_g$ | $8.6 \times 10^{-4}$ m |
| Contact angle | $\beta$ | 15 deg |
| Coefficient of friction | $\mu_s$ | 0.3 |
| Material hysteresis | $\alpha$ | 0.05% |
| Bearing normal load | $P$ | 110 N |
| Number of bearings | $n_b$ | 48 |
| Moving joint half-mass | $m_j$ | 0.034 kg |
| Distance from the rotation axis to the center of gravity | $r_{cg}$ | 0.0118 m |

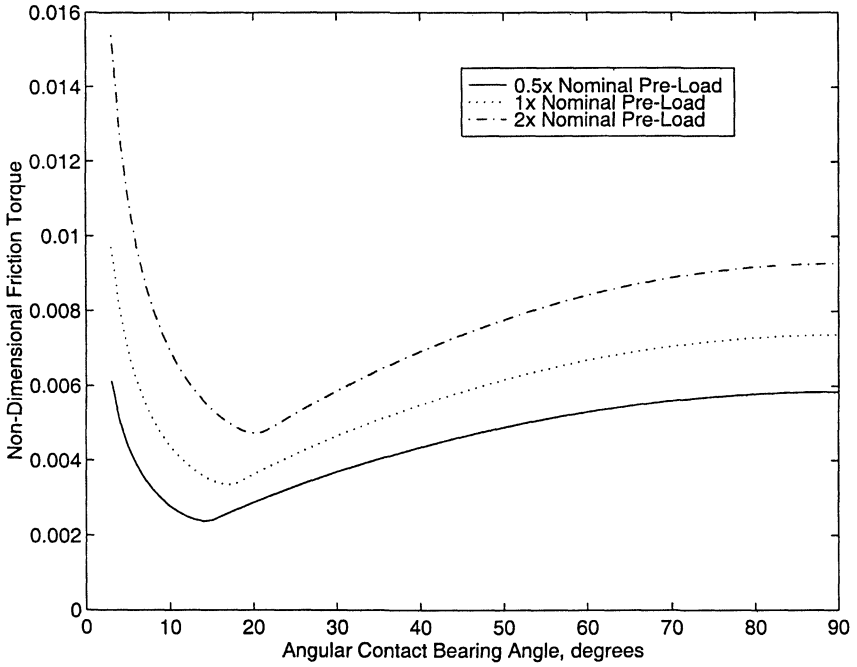


**Fig. 10 Nondimensional friction torque as a function of angular contact bearing angle graph.**

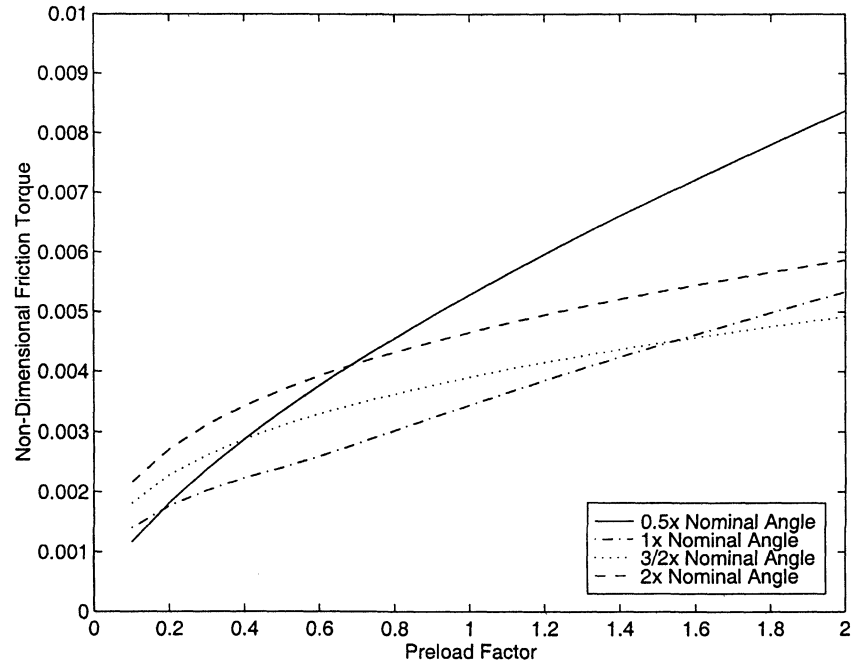


**Fig. 11 Nondimensional friction torque as a function of preload.**

the nominal (1 × preload) preload curve, the minimum torque occurs when the angular contact bearing angle is ~17 deg. That the nominal bearing angle is 15 deg means that the nominal design is near the minimum friction for this bearing.

The relationship between preload and the nondimensional friction torque for a given nominal angular contact bearing angle (for this example, the nominal angular contact bearing angle is 15 deg) is shown in Fig. 11. These curves represent the minimum friction torque attainable given a preload and available angular contact bearing angle. Note that although the friction torque is a monotonically nonlinear increasing function of the preload, the slope of the function becomes more linear as the preload increases.

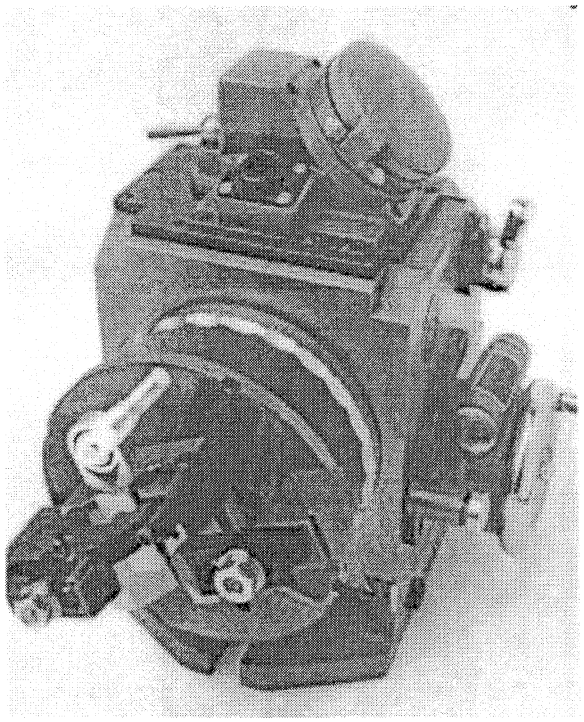

**Fig. 12 Experimental apparatus.**

## Experimental Validation of Joint Friction Torque

### Test Specimen

The model was validated by experimentally measuring the breakaway friction within the precision revolute hinge joint shown in Fig. 1. The joint is constructed with a matched pair of angular contact bearings with the physical characteristics listed in Table 1.

### Apparatus and Procedure

The experimental apparatus is shown in Fig. 12. It consists of a precision machine index head with an attachment apparatus mounted to the front of the index head. One end of the joint was mounted into the attachment apparatus on the index head, was centered, then was clamped. The other end of the joint remained free to rotate. Centering of the joint consisted of determining that the two halves of the joint were aligned about the same vertical axis. As part of the centering procedure, the rotation axis of the joint was positioned to be perpendicular to the plane of the mounting face of the index head. An electronic level, with a resolution of 0.1 deg, was used in the alignment process.

Once the joint was aligned, the index face was manually rotated counterclockwise at approximately ~2 deg/s. At a critical angle, the gravity torque on the joint overcomes the friction torque. Torque equilibrium about the rotation axis determines that this angle would be the following:

$$T_{ss} = r_{cg} m_j g \sin\theta \tag{41}$$

Numerical values required for data reduction are presented in Table 1. Once the breakaway angle was reached, rotation of the index head ceased, and the angle of the index head was measured using the electronic level. The procedure was repeated 30 times.

### Experimental Results

The experimental data are presented in Fig. 13. The mean breakaway angle was 54.2 deg. This angle value corresponds to $T_{ss} = 0.45$ oz-in. The analytical model predicted a friction torque of 0.50 oz-in. A perturbational analysis was performed to understand the sensitivity of the torque model to variances of the physical parameters. There is an 11.5% error between the predicted and measure friction torques, which can be explained by a 10% uncertainty in actual preload force and friction coefficient value due to irregular surface finish, presence of debris, and difficulty in identifying specific steel type.

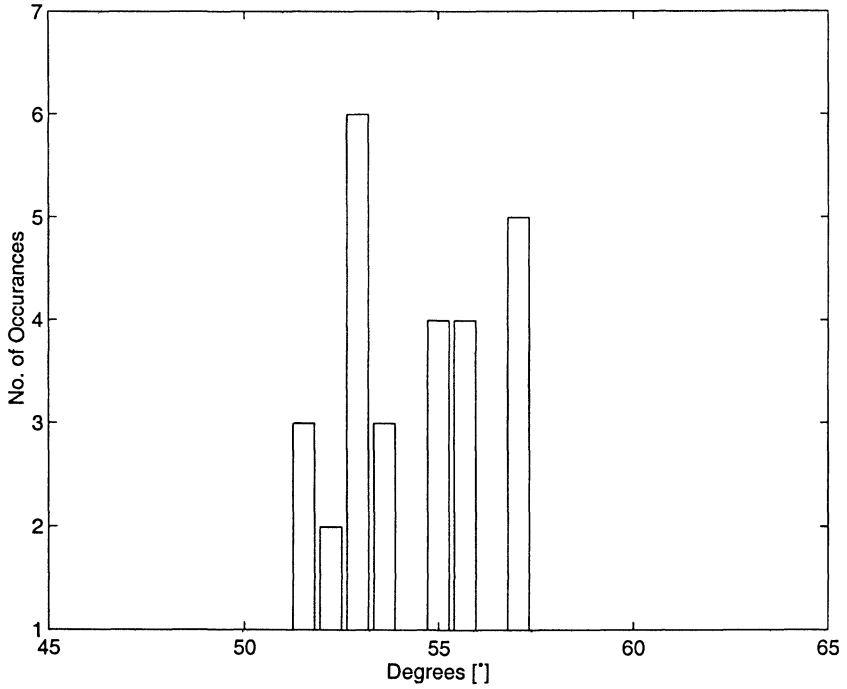


**Fig. 13 Angle at which joint rotated test results.**

## Conclusion

This paper presents an analytical model for predicting friction torque in a precision deployable spacecraft structure joint incorporating preloaded angular contact bearings. The model is based on the Todd/Johnson[21] tribological friction model of friction within ball bearings, which had previously only been validated in simple three-ball bearings. More importantly, a new nondimensional parameter has been developed to quantify the effects of bearing preload, geometry, and material properties. It is shown that friction is minimized for a specific bearing contact angle that minimizes both rolling and sliding friction components. Additionally, it is shown how friction varies nonlinearly with preload. Experimental measurements of the breakaway friction torque are compared to the analytical prediction. The error between the predicted and actual friction torques is shown to be within the uncertainty of the properties of the bearings.

## Appendix: Hertzian Contact

Hertz[24] developed a theory to predict the stress field created when two elastic bodies are statically compressed together. By assuming each body behaves as an elastic half-space and by neglecting tangential shear stress at the contact interface, the resulting contact area is an ellipse with a pressure distribution given by

$$p(x, y) = p_0[1 - (x/a)^2 - (y/b)^2]^{\frac{1}{2}} \tag{A1}$$

where $x$ and $y$ are coordinate axes centered in the contact ellipse and $p_0$ is the maximum pressure, which occurs at the center of the contact ellipse. Integrating Eq. (A1) across the contact ellipse gives the following relationship between maximum pressure $p_0$ and the total resultant force $P$ due to the contact pressure:

$$p_0 = 3P/2\pi ab \tag{A2}$$

Using the analysis of Timoshenko and Goodier,[25] the semimajor dimension is

$$b = \sqrt[3]{\left(\frac{3\pi}{2}\right)\frac{Pkr_g r_b}{(r_g - r_b)}} \tag{A3}$$

and the semiminor axes for the inner and outer contact ellipses, $a_i$ and $a_o$, respectively, are

$$a_i = \sqrt[3]{\left(\frac{3\pi}{2}\right)\frac{Pkr_b R_i}{(r_b - R_i)}}, \qquad a_o = \sqrt[3]{\left(\frac{3\pi}{2}\right)\frac{Pkr_b R_o}{(R_o - r_b)}} \tag{A4}$$

## Acknowledgments

This research was supported by NASA Training Grant NTG-10033 under the University Space Engineering Research Center Fellowship Program, by the NASA In-Space Technology Experiments Program through Contract NASW-4873, by NASA Langley Research Center through Grant NAG1-1700 with Marvin Rhodes as Technical Monitor, and by NASA Langley Research Center through Grant NAG1-1840.

## References

[1]Sathyanarayan, M. N., Nageswara Rao, M., Nataraju, B. S., Viswanatha, N., Laxmana Chary, M., Balan, K. S., Sridhara Murthy, V., Aller, R., and Suresha Kumar, H. N.,"Insat-2A & -2B Deployment Mechanisms," *Proceedings of the 28th Aerospace Mechanisms Symposium*, NASA CP-3260, 1994, pp. 17–34.

[2]Fiore, J., "Mechanical Design and Verification of the Topex/Poseidon Deployable Solar Array," AIAA Paper 94-1323, May 1994.

[3]Herald, M., and Wai, L. C., "Two-Axis Antenna Positioning Mechanism," *Proceedings of the 28th Aerospace Mechanisms Symposium*, NASA CP-3260, 1994, pp. 183–198.

[4]Batista, J., Vise, J., and Young, K., "Roll Ring Assemblies for the Space Station," *Proceedings of the 28th Aerospace Mechanisms Symposium*, NASA CP-3260, 1994, pp. 35–50.

[5]Brunschvig, A., "Pointing and Tracking Space Mechanism for Laser Communications," *Proceedings of the 28th Aerospace Mechanisms Symposium*, NASA CP-3260, 1994, pp. 211–228.

[6]O'Brien, D. L., "International Space Station Alpha's Bearing, Motor, and Roll Ring Module Development Testing and Results," *Proceedings of the 28th Aerospace Mechanisms Symposium*, NASA CP-3260, 1994.

[7]Peterson, L. D., Lake, M. S., Bullock, S. J., Hachkowski, M. R., Hinkle, J. D., and Warren, P. A., "Micro Accurate Deployable Antenna and Sensor Technology for New-Millennium-Era Spacecraft," *Proceedings of the 1996 IEEE Aerospace Applications Conference*, Inst. of Electrical and Electronics Engineers, Piscataway, NJ, 1996, pp. 129–139.

[8]Lake, M. S., Warren, P. A., and Peterson, L. D., "A Revolute Joint with Linear Load-Displacement Response for Precision Deployable Structures," *Proceedings of the AIAA/ASME/ASCE/AHS/ASC 37th Structures, Structural Dynamics, and Materials Conference*, AIAA, Reston, VA, 1996, pp. 1639–1647.

[9]Warren, P. A., and Peterson, L. D., "Experimental Characterization of the Nonlinear Postdeployment Micromechanics of Precision Deployable Space Structures," *Proceedings of the AIAA/ASME/ASCE/AHS/ASC 37th Structures, Structural Dynamics, and Materials Conference*, AIAA, Reston, VA, 1996, pp. 2364–2373.

[10]Bullock, S. J., and Peterson, L. D., "Nonlinear Micron-Level Mechanics of a Precision Deployable Space Structure Joint," AIAA Paper 96-1333, April 1996.

[11]Warren, P. A., "SubMicro Non-Linear Shape Mechanics of Precision Deployable Structures," Ph.D. Dissertation, Dept. of Aerospace Engineering Sciences, Univ. of Colorado, Boulder, CO, July 1996.

[12]Fusaro, R. L., "Government/Industry Response to Questionnaire on Space Mechanisms/Tribology Technology Needs," NASA TM-104358, May 1991.

[13]Campbell, B. E., and Hawkins, W., "An 11-Meter Deployable Truss for the Seasat Radar Antenna," *Proceedings of the 12th Aerospace Mechanisms Symposium*, NASA CP 2080, 1978, pp. 77–88.

[14]Johnson, K. L., "The Effect of Spin Upon the Rolling Motion of an Elastic Sphere on a Plane," *Journal of Applied Mechanics*, Vol. 25, Sept. 1958, p. 332–338.

[15]Halling, J., "The Microslip Between a Ball and Its Track in Ball-Thrust Bearings," *Journal of Basic Engineering*, Vol. 88, March 1966, pp. 213–220.

[16]Halling, J., "The Microslip Between a Rolling Element and Its Track Arising from Geometric Conformity and Applied Surface Tractions," *Journal of Mechanical Engineering Science*, Vol. 6, No. 1, 1964, pp. 64–73.

[17]Heathcote, H. L., "The Ball Bearing: In the Making, Under Test and on Service," *Proceedings of the Institute of Automobile Engineers*, Vol. 15, 1921, p. 569.

[18]Tabor, D., "The Mechanism of Rolling Friction: The Elastic Range," *Proceedings of the Royal Society of London*, Vol. A229, Plate 6, 1955, pp. 198–220.

[19]Palmgren, A., "Sliding Friction in Ball Bearings," *Engineering*, Vol. 107, 1919, p. 289.

[20]Poritsky, H., Hewlett, C. V., and Coleman, R. E., "Sliding Friction of Ball Bearings of the Pivot Type," *Journal of Applied Mechanics*, 1947, pp. 261–268.

[21]Todd, M. J., and Johnson, K. L., "A Model for Coulomb Torque Hysteresis in Ball Bearings," *International Journal of Mechanical Science*, Vol. 29, 1987, pp. 339–354.

[22]Dahl, P. R., "A Solid Friction Model," The Aerospace Corp., AFO 4695-67-C-D158, El Segundo, CA, May 1968.

[23]Johnson, K. L., *Contact Mechanics*, Cambridge Univ. Press, Cambridge, England, UK, 1985.

[24]Hertz, H., "Uber Die Beruhurung Fester Elasticher Korper," *Journal Reine und Angewandte Mathematick*, Vol. 92, 1881, pp. 156–171.

[25]Timoshenko, S. P., and Goodier, J. N., *Theory of Elasticity*, McGraw–Hill, New York, 1951, pp. 372–377.

R. B. Malla
*Associate Editor*